2026

# Prospectivity Mapping for Granite-related Tin-Tungsten-Fluorine-Rubidium Mineral Systems in Tasmania

Author: T. Czertowicz
Date: 10/04/2026
Email: info@mrt.tas.gov.au
Website: www.mrt.tas.gov.au

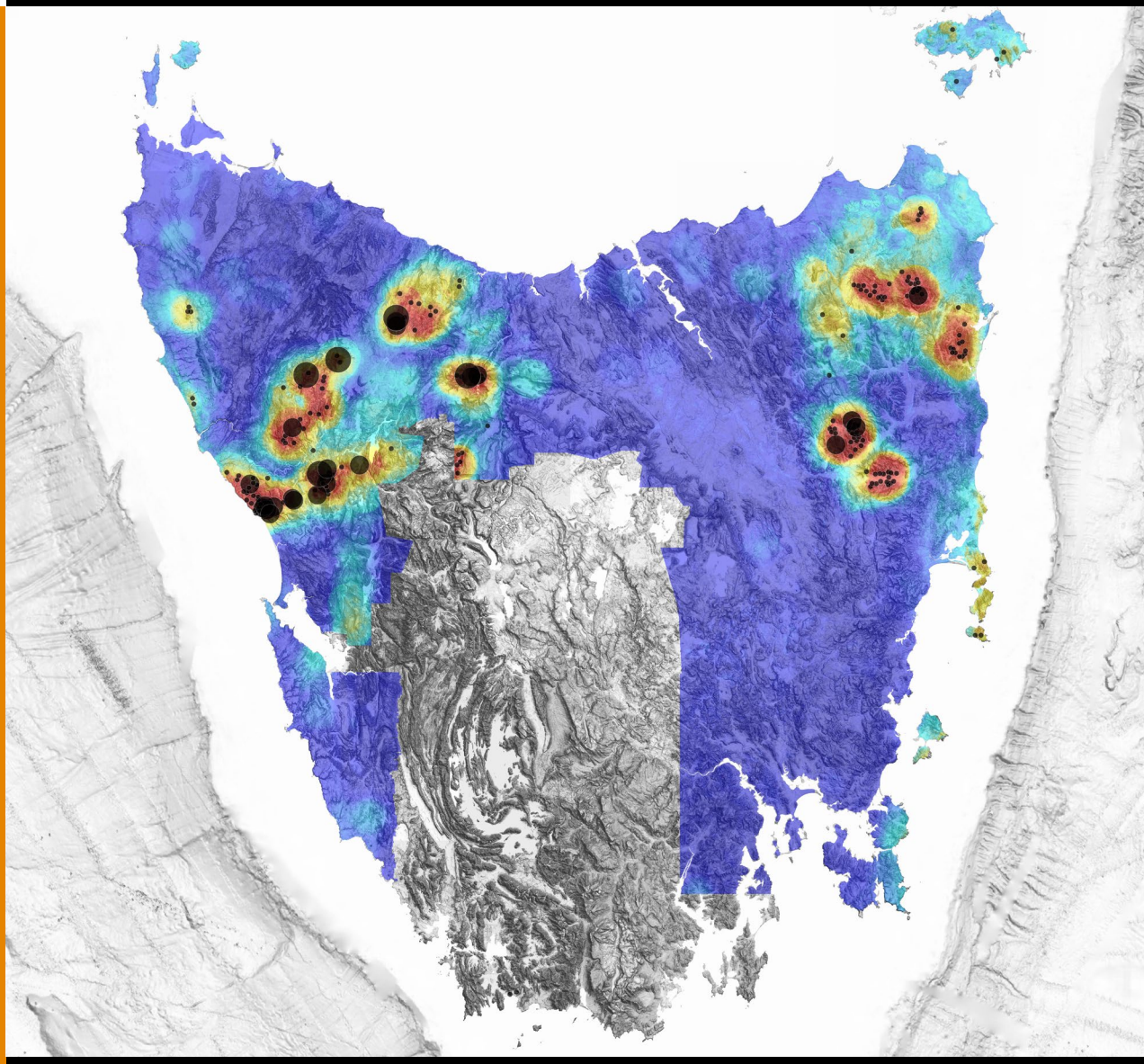

REPORT No.: TR48

Geological Survey
Technical Report 48

Tasmanian Government

# Geological Survey Technical Report 48:

## Prospectivity Mapping for Granite-related Tin-Tungsten-Fluorine-Rubidium Mineral Systems in Tasmania

by
T. Czertowicz

Cover: Statewide granite-related tin-tungsten-fluorine-rubidium prospectivity snapshot.

# Executive Summary

This report presents machine learning-based prospectivity mapping for granite-related tin-tungsten-fluorine-rubidium (Sn-W-F-Rb) mineralisation across Tasmania, supporting the Tasmanian Government's Critical Minerals Strategy by identifying high-potential exploration targets for strategic and critical minerals essential to future technologies.

The modelling used a mineral system approach, which considers the large-scale processes that co-occur within the crust to form mineral deposits. Predictor maps were generated that represent each source, transport, trap, and deposition process. Random forest machine learning was applied to integrate geological, geophysical, and geochemical datasets at 40 m resolution across the state. Two models were developed: (1) a geophysics-only model suitable for regional and greenfield targeting, and (2) a comprehensive model incorporating all available data for refined exploration targeting. Models were trained on 210 known deposits and validated using several independent techniques and expert geological feedback within Mineral Resources Tasmania.

Both models demonstrate excellent performance, capturing 90% of known deposits within the top 7-9% most prospective areas. Spatial cross-validation confirms the models can reliably predict prospectivity in new, unexplored regions. High prospectivity areas are concentrated in northwest and northeast Tasmania, corresponding to Devonian-Carboniferous granites, with almost all known deposits plotting within highly prospective zones.

The most important predictor maps are consistent with the granite-related Sn-W-F-Rb mineral system model, including proximity to fractionated granites, residual gravity lows, and pathfinder geochemistry (tin, tungsten, rubidium, molybdenum). Several areas show high prospectivity but lack documented deposits, including northern Flinders Island and the Tasman Peninsula, representing potential targets for follow-up exploration.

These models reduce exploration search space by over 90%, providing objective, data-driven evidence to improve exploration efficiency and inform land-use decisions. Results will guide resampling of legacy drill core to determine the critical mineral budgets of these systems. The methodology will be extended to other critical mineral-bearing systems across Tasmania with models updated as new data become available.

Tasmanian Government

Mineral Resources Tasmania www.mrt.tas.gov.au Department of State Growth

# Prospectivity Mapping for Granite-related Tin-Tungsten-Fluorine-Rubidium Mineral Systems in Tasmania

by T. Czertowicz
*Geological Survey Branch - Mineral Resources Tasmania*

CONTENTS

## FIGURES



## TABLES

## 1.0 INTRODUCTION

This report presents prospectivity mapping for granite-related tin-tungsten-fluorine-rubidium (Sn-W-F-Rb) mineralisation across Tasmania using machine learning, a mineral systems approach, and diverse geoscientific datasets to identify areas of high mineral potential.

This work supports global efforts to identify and develop critical mineral resources to support future technologies and the green energy transition. The Tasmanian Government's Critical Minerals Prospectus highlights Tasmania's unique position in the world in hosting a diverse range of critical minerals alongside access to high-quality infrastructure and abundant renewable energy. A key objective of the Government's Critical Minerals Strategy is to grow exploration for these commodities.

To achieve this, Mineral Resources Tasmania is developing a series of statewide prospectivity models for critical mineral-bearing systems. These models will promote investment, support exploration companies to target effectively, and provide strategic input into land use decision making. The models will also be used to identify legacy drill core stored at the Mornington Core Library for resampling using modern analytical techniques to drive new discoveries across the state.

This pilot study focused on granite-related tin-tungsten-fluorine-rubidium mineralisation, which is well studied in Tasmania and hosts significant defined resources of strategic and critical minerals. Tin is a strategic metal used primarily in electronics and soldering, tungsten is a critical mineral used for defence and aerospace applications, fluorine, also a critical mineral, is used for propulsion systems, electronics, and battery production, and rubidium is used in military applications, including night goggles, and emerging quantum technologies. The pilot study develops the methodology and workflows that will be applied to other critical mineral-bearing systems in Tasmania. The modelling results both validate current understanding by highlighting known mineralised areas and identify areas of previously unrecognised potential.

## 2.0 GEOLOGICAL SETTING AND TARGET MINERAL SYSTEM

Tasmania comprises two distinct terranes referred to as Western and Eastern Tasmania (Baillie, 1985). The division between the terranes is obscured by Mesozoic sediments and associated dolerite sills that cover much of the Precambrian to Carboniferous basement rocks. Western Tasmania includes Mesoproterozoic marine sedimentary successions and their deformed and metamorphosed equivalents, a Cambrian ophiolite allochthon, a post-collisional volcanic belt, Cambrian to Ordovician siliciclastics, and Devonian granites (Berry et al., 2025). Eastern Tasmania comprises Ordovician deep-water flysch deposits intruded by voluminous granite batholiths. In the Middle Devonian, both terranes were deformed during the Tabberabberan Orogeny at c. 389 Ma (Black et al., 2005). This event likely corresponds to the suturing of the two terranes (Black et al., 2010).

Most granites in Tasmania were emplaced during the period following the Tabberabberan Orogeny, largely between 400 and 351 Ma, at high crustal levels (Corbett et al., 2014). In Eastern Tasmania, large granitic batholiths were intruded in the Devonian (c. 400-370 Ma), whereas in Western Tasmania, smaller intrusions were emplaced in the Late Devonian to Early Carboniferous (c. 373-351 Ma) (Corbett et al., 2014). The Granites intruded the Mathinna Supergroup in Eastern Tasmania, which comprises Ordovician to Early Devonian turbidite deposits. In the west, granite was emplaced into more variable successions of Precambrian to Early Devonian age. Compositions range from granodiorite to alkali-feldspar granite, with granodiorite being more abundant in Eastern Tasmania. Both I-type and S-type granites occur in both terranes, and many intrusions are moderately to strongly fractionated.

### 2.1 Granite-related Sn-W-F-Rb

Tin-tungsten-fluorine-rubidium mineralisation worldwide occurs predominantly in greisen, vein, and replacement deposits, typically in continental or island arc settings, inboard of porphyry-skarn systems. These deposits

are commonly associated with the cupolas of highly fractionated S-type or A-type granites. Tin solubility in granitic melts is primarily controlled by oxidation state. More reduced magmas (typically S-type) concentrate tin in the melt phase, resulting in enrichment during fractionation (Corbett et al., 2014). Tungsten is less sensitive to oxidation state but is also concentrated during fractionation.

While tin and tungsten are the primary commodities, these systems may also contain critical minerals including fluorine, rubidium, bismuth, molybdenum, tantalum, lithium, and caesium. These minerals are increasingly important for future technologies and are being considered for co-processing to add value to projects.

Tin deposits in Tasmania are associated with both S- and I-type granites, although the I-type granites are more reduced than is typical worldwide (Corbett et al., 2014). Granite-related tin-tungsten-fluorine-rubidium deposits in Tasmania can be subdivided into:

1. tin (± tungsten) deposits associated with reduced and strongly fractionated I- and S-type granites, commonly associated with magnetite ± fluorite skarns; and
2. tungsten deposits associated with moderately oxidised to moderately reduced I-type granites.

Economically significant deposits are more abundant in northeast Tasmania than in the west. Northeastern granites appear to have undergone a greater degree of unroofing compared to those in the west (Corbett et al., 2014), potentially removing the more prospective apices of the intrusions. The northeast also lacks the reactive ultramafic and calcareous rocks that are common in the west. Wolframite and cassiterite vein deposits and cassiterite greisen deposits dominate in the northeast, whereas skarns and carbonate replacement deposits are more abundant in the west.

Major granite-related tin, tungsten, and fluorine deposits in Tasmania include:

- Renison tin skarn: 24.5 Mt @ 1.41% Sn (pre-mining resource; Seymour et al., 2006)
- Mount Bischoff tin skarn: 10.5 Mt @ 1.1% Sn (pre-mining resource; Seymour et al., 2006)
- Moina magnetite-fluorite skarn: 18 Mt @ 26% $CaF_2$, 0.1% Sn, 0.1% $WO_3$ (pre-mining resource; Seymour et al., 2006)
- Cleveland tin skarn: 7.47 Mt @ 0.75% Sn, 0.30% Cu (current resource; Elementos Ltd, 2026)
- Cleveland tungsten skarn: 8.5 Mt @ 0.24% $WO_3$ (current resource; Elementos Ltd, 2026)
- Queen Hill tin skarn: 4.11 Mt @ 0.85% Sn (current resource; Stellar Resources Ltd, 2026)
- King Island tungsten skarns: 11.36 Mt @ 0.90% $WO_3$ (current resource; King Island Scheelite Ltd, 2019)

## 3.0 METHODS

### 3.1 Mineral Potential Mapping

Mineral potential mapping aims to use available geoscientific data to predict the likelihood of discovering a mineral deposit at a given location. All methods essentially combine the input datasets using an algorithm to produce an output heatmap showing the relative prospectivity over a study area.

The simplest approach is to use a knowledge-driven method, such as fuzzy logic, where data layers known to map critical components of the mineral system (referred to as predictor maps) are overlain and weighted according to their importance. Data-driven methods are favoured in well-explored regions and use known examples of mineralisation (commonly deposit locations) to train the model, essentially determining the weights for each input based on the spatial correlation between the deposit training points and the predictor layer. Examples of data-driven methods include weights of evidence, logistic regression, and machine learning techniques such as random forest, support vector machines, and gradient boosting machines. This study used the random forest method, described in further detail below.

### 3.2 Mineral Systems Approach

A mineral system refers to the large-scale focussing of energy and mass flux in the crust, which results in the formation of mineral deposits (Wyborn et al., 1994). Deposit formation is dependent on deriving ore-forming components from a source, transporting and accumulating the components in a trap, depositing metals, and preserving the metals through geological time. If any of these processes are lacking, no deposit will form.

As well as metals, a source needs to provide heat, energy, and fluids, which are required to mobilise the metals. Various fluid pathways can be involved in transportation of the ore-bearing fluid including faults, shear zones, and porous rock types. Traps may be chemical, involving reactive host rocks that reduce the solubility of the metals, or physical, which typically involve focussing of large volumes of fluid through a restricted region.

The mineral system approach is particularly well-suited to mineral potential mapping since each of these critical processes can be mapped using geological proxies. It also captures the inherent variability within deposit classes, allowing various styles to be targeted in a single model.

### 3.3 Modelling Workflow

The modelling for this study was conducted over the entire state of Tasmania at a resolution of 40 m. This was chosen to match the magnetic dataset, as this represents the highest resolution input data used in the modelling. Using the finest resolution ensures that the model captures the most spatial detail possible, preserving small-scale variations which may reflect key expressions of the target mineral system. Advances in computing hardware and machine learning algorithms allow models covering large areas to be run at high spatial resolution within practical timeframes. A workflow was developed for the prospectivity mapping which involved the following major steps:

1. Review of the mineral system and determination of likely important predictor maps.
2. Compilation of relevant geological, geophysical, and geochemical datasets.
3. Selection and weighting of training points.
4. Preparation of predictor maps using GIS methods.
5. Modelling using Random Forest to produce output prospectivity maps
6. Validation of the output maps

The final two steps were iterated to produce the most geologically reasonable and practically useful output.

Datasets used for the modelling were sourced from Mineral Resources Tasmania and Geoscience Australia and included 1:250 000 geology mapping (including folds, faults, contacts, and unit polygons); several geophysical datasets including a DEM, gravity, magnetics, magnetotellurics, and radiometrics; as well as rock chip, drillhole, and mineral occurrence databases (Table 1).

QA/QC was conducted on all input data prior to modelling, which included verification of spatial alignment and coordinate systems in GIS, validation of geometries, review of geological attributes, and removal of duplicates and invalid geochemical values. All input data were standardised to a common model grid and coordinate system to ensure pixel locations matched exactly. Following this, additional attributes were compiled and numerous processing approaches were used to generate predictor maps, including buffering, density calculations, worm extraction from magnetic and gravity data, and terrain texture analysis.

### 3.4 Training Data

Hard-rock granite-related tin, tungsten, and fluorine deposits were used as positive training points for the modelling. A total of 210 deposit locations were extracted from the mineral occurrence database. Training data were weighted to ensure that the largest deposits have greatest influence over the model since larger deposits are better understood and represent the primary targets for explorers. Weights ranged from 1 to 3, corresponding to very small to very large deposit classifications in the database.

Negative training points were generated randomly across the study area, excluding any locations within a 1 km buffer around known

deposits to avoid labelling prospective ground as unprospective. An equal number of negative training points were generated and assigned a weight of 1. This ratio of 1:1 was chosen to address class imbalance, which is often present in mineral potential mapping due to deposits representing relatively rare features.

### 3.5 Predictor Maps

The mineral system approach was used to define 106 predictor maps representing proxies for the key components (Table 2; Figure 1). Each map represents either a source, transport, trap, or deposition process that may have occurred during mineralisation.

These maps were tested in various iterations of the modelling, with the most effective and geologically sound predictors retained in the final models. Known predictors of regional-scale granite-related Sn-W-F-Rb mineralisation in Tasmania that informed predictor map generation include proximity to Devonian-Carboniferous granites, highly fractionated granite compositions, presence of reactive host rocks, gravity lows (mapping buried granites), and radiometric anomalies (mapping surface granite expression).

Some datasets required minimal processing and could be used directly, such as certain gravity and magnetic grids. Derivatives of geophysical data were generated including upward and downward continuations and worm analysis to enhance horizontal gradients.

Proximity-based predictor maps were created by buffering datasets including faults, source rocks, and geochemical anomalies. Queries were commonly applied to source datasets prior to buffering to isolate specific features of interest (e.g., orientations of faults, fractionated granites). A density map was also created from the fault dataset to quantify deformation intensity (Figure 1).

**Table 1.** Datasets used for the modelling.

| Dataset | Source | Download Link |
|---|---|---|
| 1:250,000 Geology (polygons, faults, contacts, linears) | Mineral Resources Tasmania | https://www.mrt.tas.gov.au/products/digital_data/data_downloads/geology_of_tasmania |
| Mineral Occurrences | Mineral Resources Tasmania | https://www.mrt.tas.gov.au/products/digital_data/data_downloads/mineral_occurrences_data |
| Mineral Drillholes | TIGER database | https://www.mrt.tas.gov.au/products/digital_data/data_downloads/boreholes_drill_holes_data |
| Rockchip samples | TIGER database | https://www.mrt.tas.gov.au/products/digital_data/data_downloads/samples_and_observations_data |
| Magnetotellurics | AusLAMP | https://ecat.ga.gov.au/geonetwork/srv/eng/catalog.search#/metadata/149489 |
| Magnetics | Mineral Resources Tasmania | https://www.mrt.tas.gov.au/products/digital_data/data_downloads/geophysics_data |
| Gravity | Mineral Resources Tasmania | https://www.mrt.tas.gov.au/products/digital_data/data_downloads/geophysics_data |
| Radiometrics | Mineral Resources Tasmania | https://www.mrt.tas.gov.au/products/digital_data/data_downloads/geophysics_data |
| DEM | Mineral Resources Tasmania | N/A |
| Modelled Devonian granite upper surface | Mineral Resources Tasmania | N/A |

**Table 2.** Mineral system components incorporated into the modelling.

| Granite-related Sn-W-F-Rb | | | |
|---|---|---|---|
| **Source:**<br>• Granites<br>• Fractionated Granites<br>• Granite cupolas<br>• Gravity anomalies<br>• Magnetic anomalies<br>• Radiometric anomalies<br>• MT anomalies | **Transport:**<br>• Faults<br>• Fault orientations<br>• Contacts<br>• Gravity worms<br>• magnetic worms | **Trap:**<br>• Magnetic anomalies<br>• Contacts<br>• Reactive rocks<br>• Fault intersections<br>• Fault density<br>• Folds | **Deposition:**<br>• Geochemical anomalies<br>• Mineral occurrences |

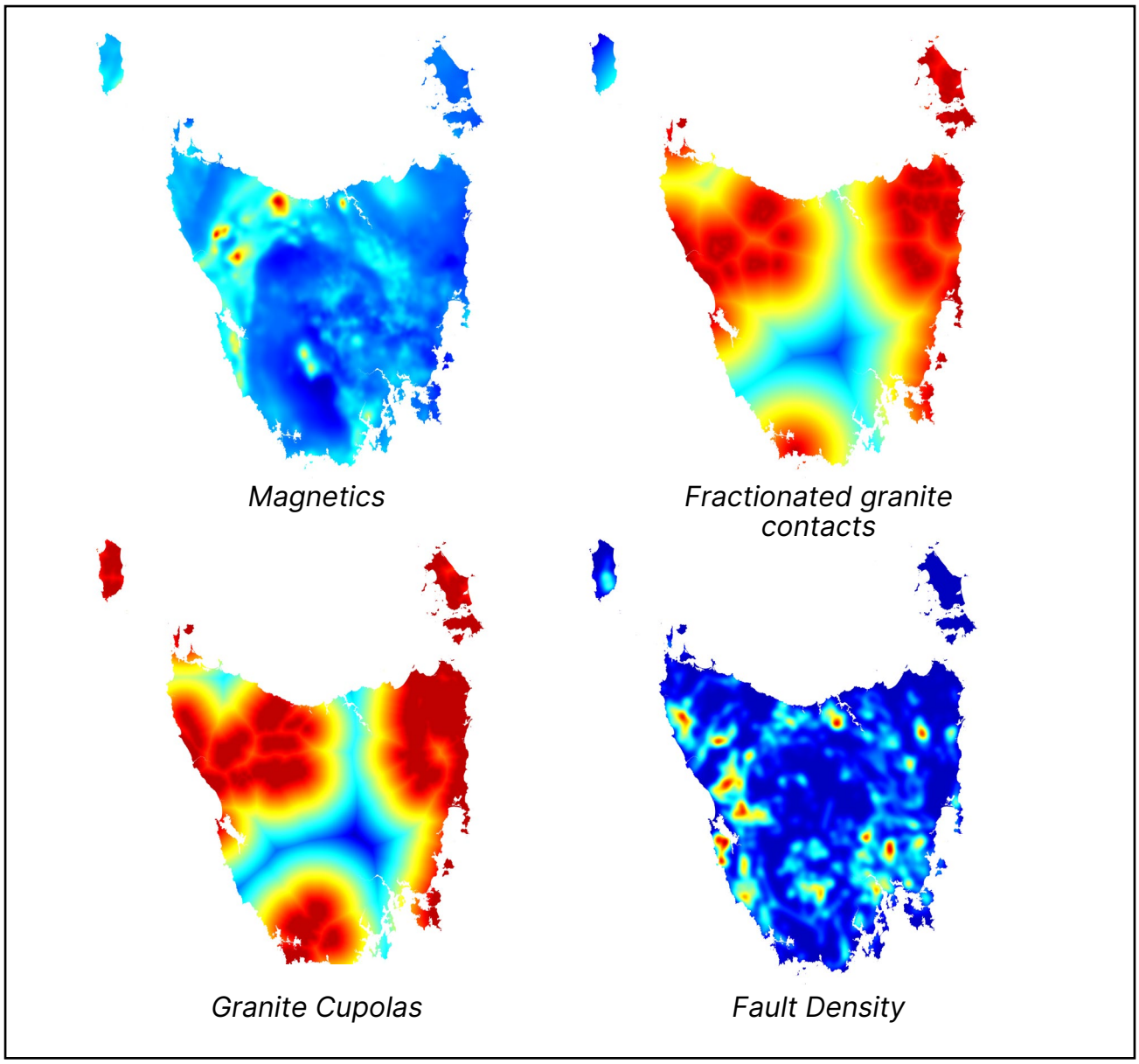


**Figure 1.** Example predictor maps used as inputs for the random forest modelling.

Geochemical anomalies were determined through whole-dataset statistical analysis using the ioGAS software package. Threshold values were selected using a combination of probability plots and consideration of percentiles.

Texture analysis of geophysical datasets was performed using the Gray-level Co-occurrence Matrix (GLCM) method. This analysis compares pixel values within a chosen search window and provides metrics such as contrast and entropy that characterise textural variations in the data.

### 3.6 Random Forest

Random forest (Breiman, 2001) is a machine learning algorithm that has been successfully applied to mineral potential mapping applications in various settings (Carranza and Laborte, 2015; Ford, 2020; Zhang et al., 2022; Kreuzer et al., 2025) It is particularly well suited to geological applications due to its ability to handle sparse training data, spatially correlated and missing data, as well as its computational efficiency and reproducibility. Random forest also outputs measures of variable importance, indicating which maps contributed most to the classification. This allows assessment of whether the model is operating in a geologically reasonable manner by highlighting which inputs are driving the predictions. Decision tree thresholds can also be extracted and analysed to verify they are geologically meaningful. This interpretability contrasts with “black box” approaches such as deep neural networks, where such insights can be difficult or impossible to obtain.

Random forest implementation occurs in two stages: training and classification. During training, known mineral deposits and nominal non-deposit locations are used to learn which combinations of input maps best discriminate deposits from non-deposits. The algorithm generates multiple decision trees; each built from a random subset of predictor maps and a bootstrapped sample of training data. Each node in a tree applies a threshold to a specific predictor map, chosen to optimise separation between deposits and non-deposits (Figure 2). The final classification for each pixel is determined by majority vote across all trees in the forest. During the classification stage, the trained forest is applied over the entire study area. Rather than producing a binary prospectivity map, the more commonly used output in geological applications is a probability map, where values range from 0 to 1 and represent the proportion of trees that classified each pixel as prospective.

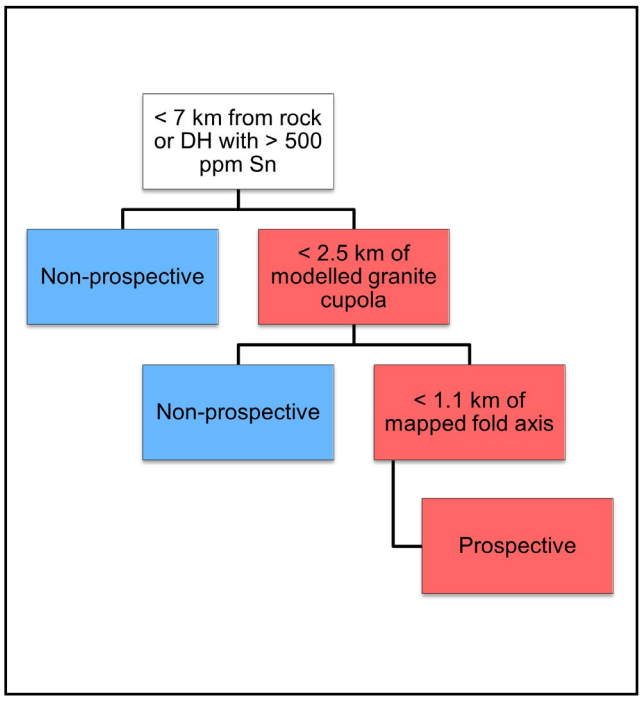


**Figure 2.** Simplified example of a tree generated during the random forest modelling.

### 3.7 Random Forest Implementation

In this study, random forest was implemented using the scikit-learn library in Python, while QGIS was used for spatial pre-processing and visualisation of results.

Hyperparameters were tuned through iterative manual testing to optimise model performance, balancing efficiency with accuracy. The final configuration was:

- Number of trees (n_estimators): 500
- Maximum tree depth (max_depth): 15
- Maximum number of features per split: square root of total
- Minimum samples per leaf (min_samples_leaf): 5
- Minimum samples per split (min_samples_split): 10

No data areas were handled differently depending on spatial extent. For small gaps in predictor map coverage, values were imputed using a separate random forest model trained on the available data for that predictor. This method uses relationships between predictor maps to estimate missing values. For larger data gaps, affected areas were masked and excluded from the analysis to avoid imputation over expansive regions. For example, there is a large gap in radiometric data over the south of the state and therefore this area was excluded from the model.

### 3.8 Validation

First-order validation of the models was conducted via expert geological feedback during meetings held at Mineral Resources Tasmania. Model predictions were compared to the current understanding of the mineral system, and any discrepancies were discussed and addressed in subsequent model iterations. This approach ensured that expert geological knowledge was systematically incorporated into the data-driven model, aligning the model result with established geological understanding of the mineral system.

Several validation metrics were generated to assess model performance. These included out-of-bag (OOB) error, standard cross-validation, and spatial cross-validation. Out-of-bag error is calculated using training data not included in the bootstrapped sample used during tree generation, providing an internal test of model accuracy. Standard cross-validation randomly splits the data into training and testing sets. However, this approach can be problematic for geological data due to spatial autocorrelation, where nearby locations can share similar characteristics, often resulting in an overestimate of model performance. Spatial cross-validation addresses this by splitting the study area

into geographic blocks. For each block, the model is trained on data from all other blocks and tested only on the held-out block. This simulates the model's ability to predict prospectivity over new or under-explored areas and provides a more realistic assessment of model performance for mineral exploration applications.

Success rate curves were plotted to visualise model efficiency. These curves show the cumulative percentage of known deposits captured as a function of the percentage of the study area, starting from the most prospective areas and moving out. The area under the curve provides a metric for comparing model performance, with higher values indicating better discrimination between prospective and non-prospective ground.

## 4.0 RESULTS

A total of 31 models were run during an iterative development process, with two selected as the final output products. These comprise one model using only geophysical data inputs (Model 1) and another using maps derived from all data types (Model 2). The goal of this two-model approach was to investigate the difference in output using only objective, continuous, and quantitative geophysical data versus including geological and geochemical maps which may contain biases related to mapping coverage, sampling density, or geological interpretations.

A list of predictor maps included in the two models is provided in Table 3. The selection of maps was based on their relevance to the mineral system, performance in previous model iterations, and their ability to capture unique map patterns.

Variable importance scores, which indicate the contribution of each predictor to the models, are also presented in Table 3, with the top predictors for Model 2 shown in Figure 3. These scores were calculated using Gini importance, which quantifies the total reduction in node impurity (i.e., improvement in the separation of prospective and non-prospective classes) attributed to each predictor across all decision trees in the random forest. Higher scores therefore indicate predictors that more effectively differentiate between prospective and non-prospective areas.

For Model 1, the maps with the highest importance were all derived from gravity datasets. Specifically, the granite cupola model (derived from residual gravity measurements) contributed the most to the model. The uranium channel radiometric map also had a significant contribution. The 39.5 km magnetotelluric depth slice and a textural measure of the DEM had moderate contributions, while all magnetic maps had limited influence.

Model 2 is largely dominated by geochemical maps with tin, rubidium, molybdenum, and tungsten all having large contributions. The granite cupola model remained important, as did a map showing proximity to fractionated Devonian to Carboniferous granites. Geophysics maps had a much lower influence than in Model 1.

### 4.1 Performance Metrics

Model performance metrics are shown in Table 4. Model 1 achieved an out-of-bag (OOB) accuracy of 0.88, a standard cross-validation accuracy of 0.88, and a spatial cross-validation accuracy of 0.81 ± 0.11. Model 2 achieved an OOB accuracy of 0.90, a standard cross-validation accuracy of 0.91, and a spatial cross-validation accuracy of 0.90 ± 0.06.

The agreement between OOB and standard cross validation scores indicates that the models are not over-fitting to the training data. The decrease between standard and spatial cross-validation is expected due to spatial autocorrelation, where nearby locations share similar characteristics, causing standard cross-validation to overestimate accuracy. Model 2 shows only a small decrease, suggesting greater predictive power in new spatial regions.

Both models demonstrate very good to excellent model performance, with Model 2 showing improved accuracy and spatial generalisation, likely due to the inclusion of geochemical maps that capture localised mineralisation signatures not represented in regional geophysical data.

**Table 3.** Predictor maps used in the final two models. Variable importance indicates the contribution of each map to the result and sum to 1.

| Predictor Map | Description | Variable Importance Model 1 | Variable Importance Model 2 |
|---|---|---|---|
| **GEOPHYSICS** | | | |
| Grav_Bouguer | Bouguer gravity | 0.03 | 0.01 |
| Grav_Residual | Residual gravity | 0.15 | 0.04 |
| Grav_Res_Worms_12856 | Residual gravity worms (12.86 km) | 0.03 | 0.01 |
| Geology_Granite_Cupola_d2 | Proximity to interpreted granite cupola (based on gravity data) | 0.25 | 0.11 |
| Geology_Granite_Slope_gt25_d2_V3_Imputed_GDA_V2 | Proximity to large slopes on interpreted granite cupola | 0.06 | 0.02 |
| Mag_cont_689 | Magnetic RTP upward continued to 0.7 km | 0.02 | 0.01 |
| Mag_cont_4174 | Magnetic RTP upward continued to 4.2 km | 0.04 | 0.01 |
| Mag_cont_1696 | Magnetic RTP upward continued to 1.7 km | 0.02 | 0.01 |
| Worms_Mag_GDA_07607 | Magnetic worms (7.6 km | 0.01 | 0.01 |
| Worms_Mag_GDA_13863 | Magnetic worms (13.9 km) | 0.02 | 0.01 |
| Tas_Rad_K_NegRemoved | Radiometrics - K | 0.01 | 0.01 |
| Tas_Rad_Th_Div_U_Norm | Radiometrics - Th/U | 0.02 | 0.01 |
| Tas_Rad_U_NegRemoved | Radiometrics - U | 0.06 | 0.02 |
| Rads_TC | Total count radiometrics | 0.03 | 0.02 |
| Tas_Rad_K_Div_Th_Norm | Radiometrics - K/Th | 0.01 | 0.00 |
| Tas_Rad_K_Div_U_Norm | Radiometrics - K/U | 0.01 | 0.00 |
| Tas_Rad_Th_NegRemoved | Radiometrics - Th | 0.02 | 0.01 |
| AusLAMP_24p91km | Magnetotelluric data - 24.91 km depth slice | 0.02 | 0.01 |
| AusLAMP_39p51km | Magnetotelluric data - 39.51 km depth slice | 0.05 | 0.02 |
| Clip_DEM_norm_GDA_120m_energy_win21_lvl256_nearest | Elevation GSCM energy parameter with a 21-pixel window | 0.05 | 0.01 |
| Clip_DEM_norm_GDA_120m_entropy_win21_lvl256_nearest | Elevation GSCM entropy parameter with a 21-pixel window | 0.03 | 0.02 |
| **GEOLOGY** | | | |
| Geology_FelsicInt_Dev_Frac_Cont_d2 | Proximity to fractionated Devonian to Carboniferous granites | - | 0.07 |
| Geology_Carbonates_d2 | Proximity to carbonate rocks | - | 0.01 |
| Faults_N_S_d2 | Proximity to N-S trending faults | - | 0.01 |
| Faults_Intersections_d2 | Proximity to fault intersections | - | 0.01 |
| Fault_Density_10km | Fault density | - | 0.01 |
| Folds_d2 | Proximity to fold axes | - | 0.01 |
| **GEOCHEMISTRY** | | | |
| d2_Tas_Rocks_DH_Anom__Li75 | Distance to lithium rock chip/DH anomaly | - | 0.07 |
| d2_Tas_Rocks_DH_Anom_Mo20 | Distance to molybdenum rock chip/DH anomaly | - | 0.10 |
| d2_Tas_Rocks_DH_Anom_Rb350 | Distance to rubidium rock chip/DH anomaly | - | 0.12 |
| d2_Tas_Rocks_DH_Anom_Sn500 | Distance to tin rock chip/DH anomaly | - | 0.16 |
| d2_Tas_Rocks_DH_Anom_W150 | Distance to tungsten rock chip/DH anomaly | - | 0.09 |

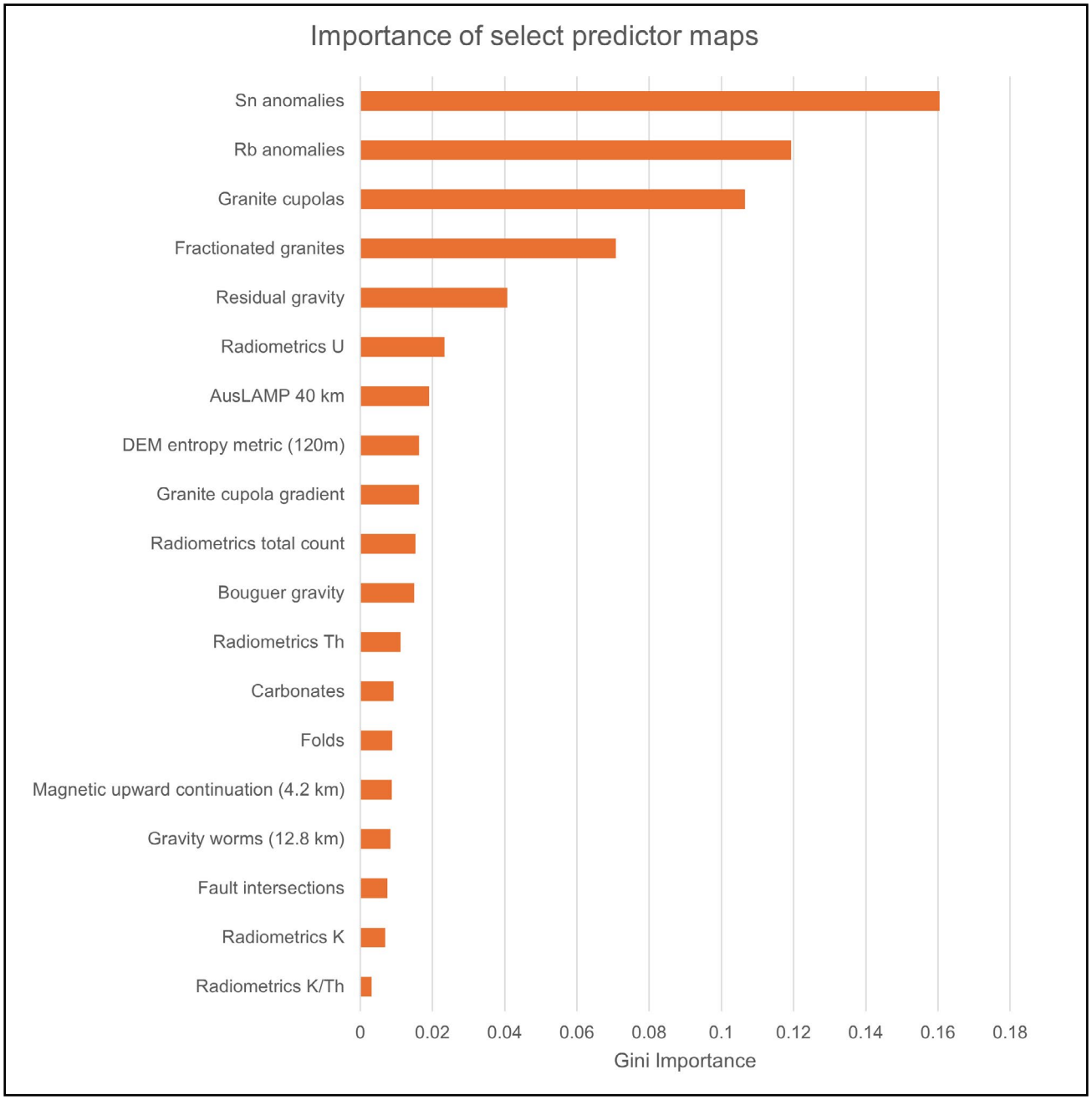


**Figure 3.** Variable importance for select predictor maps used in Model 2. Tin and rubidium anomalies had the largest contribution to the model, whereas radiometrics K/Th had little influence.

**Table 4.** Model performance metrics.

| | **Model 1** | **Model 2** |
|---|---|---|
| **Out-of-bag Score** | 0.88 | 0.90 |
| **Cross Validation Score** | 0.88 | 0.91 |
| **Spatial Cross Validation Score** | 0.81 ± 0.11 | 0.90 ± 0.06 |

Receiver Operator Characteristic (ROC) curves for the two models are show in Figure 4. These curves represent the ability of the model to separate prospective from non-prospective areas, with a perfect model hugging the top-left corner and a random classifier producing a diagonal 45° line. Model discrimination can be quantified by calculating the area under the curve (AUC). Model 1 has an AUC score of 0.895, while Model 2 has a slightly higher score of 0.952, indicating superior discrimination ability.

Success rate curves (Figure 5) indicate the efficiency of the models in terms of area required to capture a given percentage of known deposits. Model 1 captures 90% of the known deposits within 9% of the study area, while Model 2 achieves this within 7% of the area. Both models demonstrate excellent exploration efficiency, significantly reducing the exploration search space.

Overall, model performance metrics indicate excellent discrimination between prospective and non-prospective areas, with Model 2 showing marginal improvements over the geophysics-only approach.

### 4.2 Outputs

Output mineral potential maps are shown in Figures 6 and 7. These probability maps show the relative prospectivity for granite-related Sn-W-F-Rb mineralisation across the study area. In both models, the highly prospective areas are concentrated in the northwest and northeast of the state, corresponding to the locations of Devonian-Carboniferous granites. Almost all known deposits plot within the highly prospective areas, validating the models' ability to capture sites of known mineralisation.

Despite using different input datasets, the two models show broadly consistent spatial patterns. The key difference is that Model 2 delineates more concentrated areas of high prospectivity due to the added constraint provided by geochemistry data, which reduces false positives while emphasising known mineralisation.

Areas highlighted as prospective but lacking known deposits include northern Flinders Island and the Tasman Peninsula. These represent potential targets for future exploration, although ground-truthing is required to validate the results.

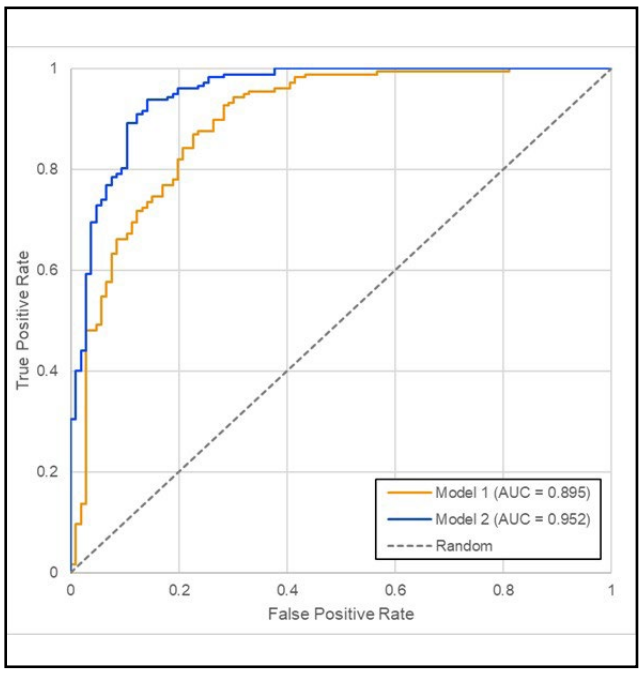


**Figure 4.** Receiver Operator Characteristic curves for the two models.

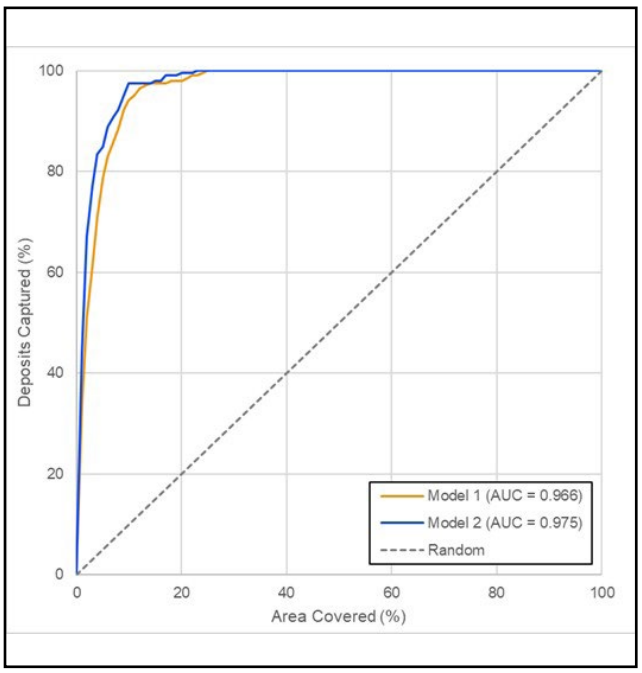


**Figure 5.** Success rate curves for the two models.

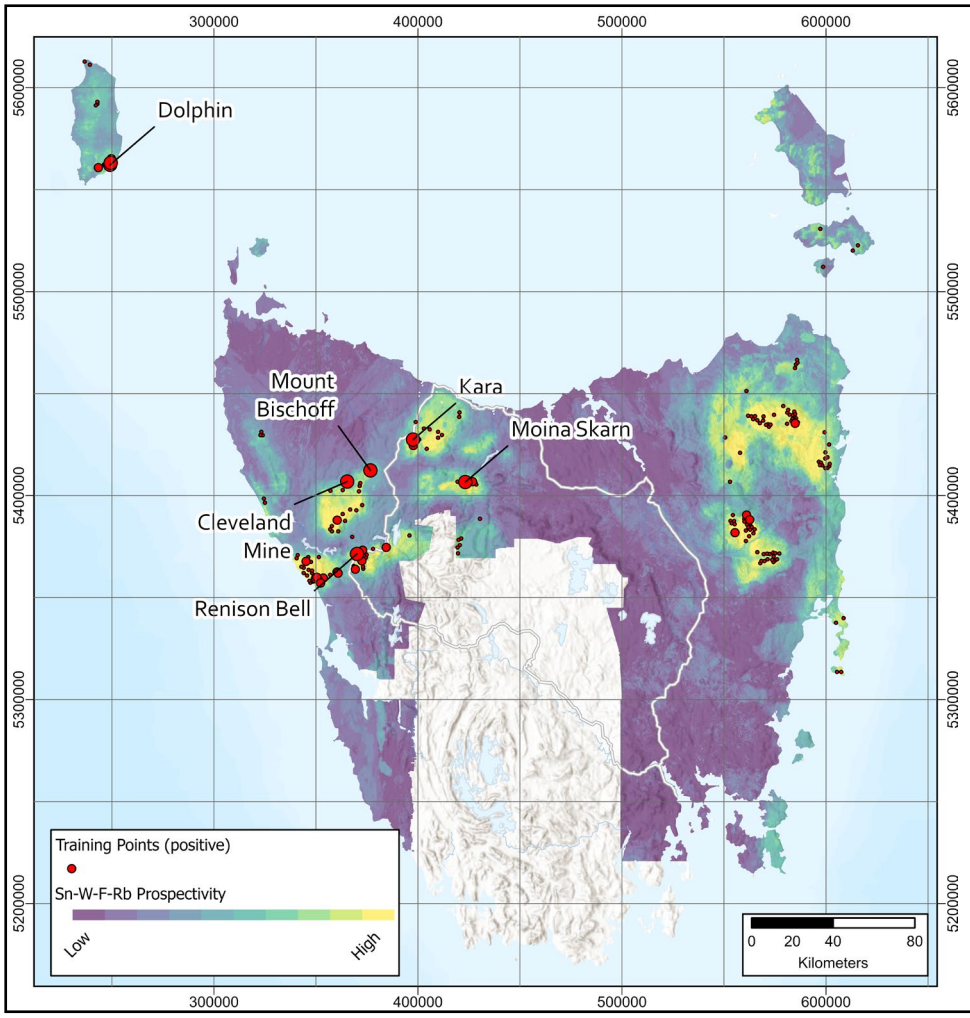


**Figure 6.** Model 1 mineral potential map showing relative prospectivity for granite-related Sn-W-F-Rb mineralisation.

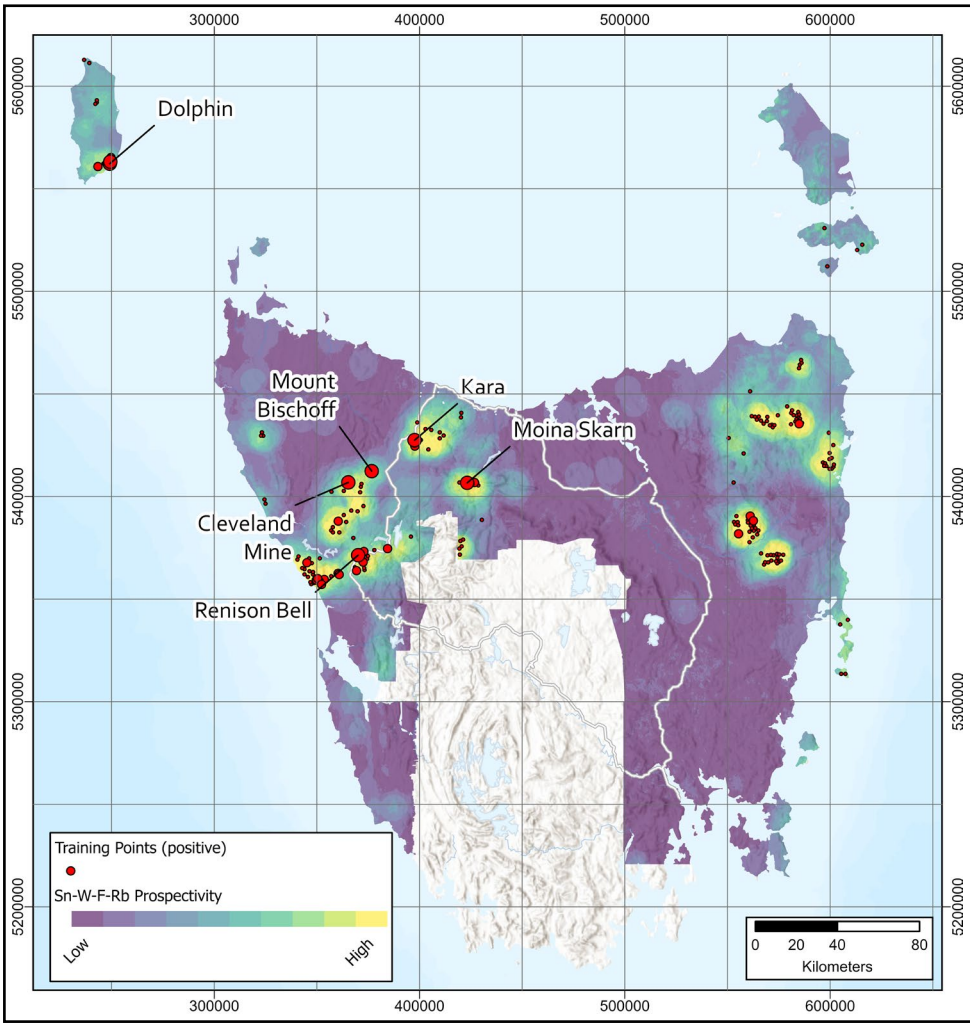


**Figure 7.** Model 2 mineral potential map showing relative prospectivity for granite-related Sn-W-F-Rb mineralisation.

## 5.0 DISCUSSION

### 5.1 Model Performance and Geological Interpretation

The methodology developed in this pilot study effectively maps known mineral potential while also predicting new exploration targets. The two-model approach provides complimentary information. Model 1 (geophysics-only) highlights regional and greenfields targets based on objective and continuous datasets, while Model 2 incorporates all available data to refine targeting to highlight only the areas most likely to host mineralisation.

The variables selected by the random forest algorithm are consistent with the granite-related Sn-W-F-Rb mineral system model. High-importance predictors broadly relate to the source granites (e.g., gravity lows, mapped fractionated granites, uranium radiometrics) and pathfinder geochemistry (tin, tungsten, rubidium, molybdenum). Variable importance scores can inform future exploration programs by identifying the most effective techniques for mapping this mineral system. For example, rubidium geochemistry proved to be a highly effective pathfinder element at the regional scale.

Surprisingly, carbonate units did not contribute significantly to the models despite their importance as a reactive host rock at many deposits. This likely reflects a scale issue: narrow carbonate horizons that serve as critical trap sites may not be mapped at 1:250 000 scale.

### 5.2 Novel Prospective Areas

Areas identified as prospective but lacking known deposits, such as northern Flinders Island and the Tasman Peninsula, warrant evaluation as potential exploration targets. However, these should be ground-truthed to distinguish genuine prospectivity from potential model artifacts. Several factors could explain these predictions: (1) genuine prospective geology with insufficient prior exploration, (2) geophysical signatures mimicking granite-related systems but representing different geological features, or (3) prediction bias toward data-rich areas. Field validation and integration with additional datasets would help resolve these ambiguities.

### 5.3 Limitations and Uncertainty

Several limitations should be considered when interpreting the modelling results:

*5.3.1 Data quality and coverage*

Model 2 incorporates geological datasets that contain inherent interpretative uncertainty regarding rock-type classification boundary positions. Structural data such as faults and folds suffer from similar issues and may be biased toward well-mapped areas. This was partially mitigated by using only regional-scale mapping data. Geochemical data are spatially biased, with denser sampling in areas of known mineralisation compared to greenfields or inaccessible areas. This may cause the models to under-predict prospectivity in under-explored areas.

*5.3.2 Training Data*

Positive training points may contain location errors or mineral system misclassifications, particularly for smaller or poorly understood mineral occurrences. This was mitigated by assigning higher weights to well understood deposits. The generation of random negative training points (excluding a buffer around positive points) introduces uncertainty since some points may overlap with sites of potential mineralisation. However, given the rarity of deposits and the large number of training points, the potential effect is considered small. Alternative approaches such as positive-unlabelled learning could be used to further address the issue in future models.

### 5.4 Exploration Implications

These models provide a first-order targeting tool that can reduce exploration search space by over 90%, focusing efforts on the most prospective 7-10% of the study area. The geophysics-only model is particularly valuable for greenfield exploration where geological and geochemical data are sparse, while the complete model offers refined targeting in well-characterised terranes. Users should consider data coverage and quality when interpreting model outputs, particularly in data-sparse regions where predictions are less constrained.

### 5.5 Future Work

The methodology developed here allows models to be updated rapidly as new data become available or as machine learning methods evolve. For example, acquisition of higher-resolution gravity data would likely improve model performance and could be readily incorporated to generate an updated prospectivity map. Immediate applications include using the results to guide a core resampling program aimed at determining the critical mineral budget of Tasmanian granite-related Sn-W-F-Rb systems. Future work will extend this approach to other critical mineral-bearing mineral systems across Tasmania, with ongoing refinement of the modelling workflow.

## 6.0 REFERENCES


**Baillie, P. W.** 1985. A Paleozoic suture in eastern Gondwanaland. *Tectonics*, 4:653–660.

**Berry, R. F.**, Everard, J. L., Bottrill, R. S., Meffre, S. 2025. Composition of pre- Carboniferous siliciclastic rocks in Tasmania. *Australian Journal of Earth Sciences*, 72:40-54.

**Black, L. P.**, Everard, J. L., Mcclenaghan, M. P., Korsch, R. J., Calver, C. R., Fioretti, A. M., Brown, A. V., Foudoulis, C. 2010. Controls on Devonian–Carboniferous magmatism in Tasmania, based on inherited zircon age patterns, Sr, Nd and Pb isotopes, and major and trace element geochemistry. *Australian Journal of Earth Sciences*, 57:933-968.

**Black, L. P.**, Mcclenaghan, M. P., Korsch, R. J., Everard, J. L., Foudoulis, C. 2005. The significance of Devonian–Carboniferous igneous activity in Tasmania, as derived from U–Pb SHRIMP dating of zircon. *Australian Journal of Earth Sciences*, 52:807–829.

**Breiman, L.** 2001. Random forests. *Machine Learning*, 45:5–32.

**Corbett, K. D.**, Quilty, P. G., Calver, C. R. 2014. Geological Evolution of Tasmania. Geological Society of Australia (Tasmania Division).

**Carranza, E. J. M.**, Laborte, A. G. 2015. Random forest predictive modeling of mineral prospectivity with small number of prospects and data with missing values in Abra (Philippines). *Computational Geosciences*, 74:60–70.

**Elementos Ltd.** 2026. Significant Tungsten MRE Increase at Cleveland Tin Project. ASX Announcement, 4 February 2026, https://wcsecure.weblink.com.au/pdf/ELT/03052737.pdf.

**Ford, A.** 2020. Practical Implementation of Random Forest-Based Mineral Potential Mapping for Porphyry Cu–Au Mineralization in the Eastern Lachlan Orogen, NSW, Australia. *Natural Resources Research*, 29:267–283.

**King Island Scheelite Ltd.** 2019. 18% Increase in Tungsten Resources. ASX Announcement, 26 September 2019, https://wcsecure.weblink.com.au/pdf/KIS/02151389.pdf.

**Kreuzer, O. P.**, Bijan, R. 2025. Transforming LCT Pegmatite Targeting Models into AI-Powered Predictive Maps of Lithium Potential for Western Australia and Ontario: Approach, Results and Implications. *Minerals*, 15:397.

**Seymour, D. B.**, Green, G. R, Calver, C. R. 2006. The Geology and Mineral Deposits of Tasmania: a summary. *Geological Survey Bulletin*, 72.

**Stellar Resources Ltd.** 2026. Queen Hill Resource Up 41%, Heemskirk Tin Inventory Over 100kt. ASX Announcement, 23 February 2026, https://wcsecure.weblink.com.au/pdf/SRZ/03059533.pdf.

**Wyborn, L. A. I.**, Heinrich, C. A., Jaques, A. L. 1994. Australian Proterozoic mineral systems: essential ingredients and mappable criteria. *Australian Institute of Mining and Metallurgy Publication Series*, 5:109-115.

**Zhang, S.**, Carranza, E. J. M., Xiao, K., Wei, H., Yang, F., Chen, Z., Li, N., Xiang, J. 2022. Mineral prospectivity mapping based on isolation forest and random forest: Implication for the existence of spatial signature of mineralization in outliers. *Natural Resources Research*, 31.

Tasmanian Government

**Mineral Resources Tasmania**
PO Box 56 Rosny Park
Tasmania Australia 7018
Ph: +61 3 6165 4800

info@mrt.tas.gov.au www.mrt.tas.gov.au